Hindawi
Advances in Materials Science and Engineering
Volume 2020, Article ID 3578281, 12 pages
https://doi.org/10.1155/2020/3578281

Research Article

Characterization of Vertical Response of Asphalt Trackbed Concrete in Railway Substructure to External Loads

Bekhzad Yusupov,[1] **Yanjun Qiu**,[1] **Galibjon Sharipov**,[2] **and Chaoyang Wu**[1]

[1]*School of Civil Engineering, Southwest Jiaotong University, Chengdu, Sichuan, China*
[2]*Institute of Agricultural Engineering (440d), University of Hohenheim, Stuttgart, Germany*

Correspondence should be addressed to Yanjun Qiu; publicqiu@vip.163.com

Received 2 August 2019; Revised 20 October 2019; Accepted 26 October 2019; Published 13 March 2020

Academic Editor: Davide Palumbo

Optimizing the dynamic responses of a slab track system is a key aspect to improve the quality of a railway track structure. In this paper, numerical modelling and simulation of vertical dynamics of the railway track structure engaging the asphalt concrete in substructures were carried out. Thus, a 3D finite element (FE) model was developed. The developed model was validated by comparing its outputs, that is, acceleration with the measured ones from realistic experimental data. The good agreement between the simulated and measured data which resulted from the validation confirmed that the proposed model has a capability of simulating the complex dynamic performances of the train-track-ground system under different loading conditions. Analyses of the determined results from the simulation model performances revealed that three specific factors, which were the speed of the train, the temperature, and thickness of the asphalt concrete trackbed, mainly influenced the dynamic behavior of the railway structure. Thereby, those factors were taken into consideration while evaluating the dynamic responses and designing the asphalt concrete trackbed in railway substructures.

1. Introduction

The railway is an important mode of transportation for any nation, because of the ongoing increase in the density of population. However, the railway mode of transportation should also meet the demands of the convenience such as safety and increased travelling speed, which requires the reliability of the track structure. Compared to the traditional types of tracks, the ballastless slab track is more widely used throughout the world with several operational advantages such as lower structure height and weight, long service life and durability, less maintenance, being dust-free, better vehicle-track interaction, high stability, and ride performance. All of these come with the quality of the railway trackbed. However, as the speed of the train continues to increase, the dynamic responses of the track structure also increase. Thereafter, the excessive dynamic responses become a serious concern for the track structure and the neighbourhood [1–3]. Thereby, there is still much work to be done to optimize and improve the dynamics of the track structure [4, 5] by understanding the nature of its response to the moving loads. One of many steps towards reducing the dynamic responses of the trackbed was the engagement of asphalt concrete trackbed in a ballastless track substructure [6–8].

A number of experimental and numerical studies dedicated to assigning asphalt materials in both traditional ballasted and ballastless railway tracks were carried out. For example, Wang et al. [9] conducted a comparative analysis of different paving materials such as asphalt concrete, rubber-modified asphalt concrete, concrete, and traditional ballast material in a ballasted track structure. The study concluded that rubber-modified asphalt concrete was the most effective material in reducing a ground-borne vibration produced by trains. However, the application of the rubber-modified asphalt demands considerably high cost. Yusupov et al. [10] have also presented a numerical study to examine and predicted the difference in asphalt behaviors at high

temperatures, in the example of viscoelastic material assigned to the asphalt concrete trackbed. Liu et al. [11] have studied the effect of mastic asphalt waterproofing layer in the railway structure and indicated that the mastic asphalt layer significantly contributes to the trackbed to be waterproof and thus could considerably reduce freeze-thaw damage risk.

Recent laboratory tests conducted for long-term monitoring of asphalt trackbed material [12] have revealed the seasonal temperature changes had a significant influence on asphalt concrete trackbed behavior. Furthermore, another laboratory test has compared the differences between two different track structures with and without asphalt concrete under cyclic loading condition. The comparison showed a decrease of about 72% in the mean foundation pressure when an asphalt concrete was used [13]. In addition to these studies, Lee et al. [14] have conducted full-scale tests to assess the performance of an asphalt track system under static loading.

It is a well-known fact that asphalt material is a vital part of the pavement; however, the loading conditions and functional requirements for the pavement structure are totally different between road and railway transport systems. Therefore, new studies to learn the application of the asphalt materials in the railway structure are required. For this propose, dynamic modulus and uniaxial creep tests have been investigated to clarify a suitable mixture design and binder for the asphalt concrete in railway structures [15, 16], in terms of moisture susceptibility and permeability deformation, and fatigue cracking of asphalt concrete mixture.

According to [17], the asphalt content should be up to 0.5% greater than that considered for pavement application with air voids of 1–3%. A comparative evaluation of different structures for the trackbed, which demonstrated the combination of asphalt trackbed and subballast layer for a higher service life, based on KENTRACK software was introduced by [18]. In addition to that, the KENTRACK program is capable of determining and analyzing different material behavior of asphalt.

Li et al. [19] evaluated the possibility of applying basic oxygen furnace on asphaltic material in trackbed and analyzed the benefits of the asphalt substructure. The next and later research by Liu et al. [20] have recommended employing epoxy asphalt in the railway structure in order to achieve high fatigue cracking-resistant performance that can minimize the main distress of structures.

It can be clearly seen from the literature review above that most of previous studies on the asphalt concrete trackbed were conducted without considering the train-track-ground coupling behavior on the effectiveness (applicability of the asphalt concrete trackbed) of asphalt concrete trackbed. It is important to consider train-track-ground coupling in order to obtain more realistic dynamic responses of the asphalt trackbed under external effects like the train speed, temperature, and the thickness of the layer and to observe its effectiveness. Therefore, the main purpose of the current study was to examine the influence of external factors, in terms of different speeds of the train, thicknesses of asphalt concrete trackbed, and weather conditions, on its dynamic responses, based on the train-track-ground coupling dynamics theory. To define the dynamic responses, a 3D FE coupled model of the train-track-ground system has been developed in ABAQUS software. The developed model was validated by comparing its output, that is, acceleration with the measured one. The effects of the speeds, weather conditions, and thickness of the trackbed have been thoroughly investigated.

2. Materials and Methods

2.1. Train Model. A new 3D FE model was established in ABAQUS software, which was fully coupled of the train-track-ground system. The model included linear effects of coupling systems between the train and track and considered the rail irregularities in the domain analysis and viscoelastic behavior of asphalt material as well. One of the very common trains in China, the articulated 8-carriages CRH3 high speed of 350 $km \cdot h^{-1}$, was employed. Each train was developed based on multibody dynamics theory in ABAQUS and it was connected to the track system. The train consists of two bogies and four wheelsets (Figure 1). The train components were modelled as rigid bodies and linked via axial connectors (spring-damper elements) to represent primary and secondary suspensions. The interaction between train and track was defined via the wheel-rail contacts by means of linear Hertzian theory. In this theory, the wheel-rail interaction forces are described as a function of the relative motion between wheel and rail [21]. By using this model, only the vertical responses can be obtained and the lateral and longitudinal responses were ignored. The physical geometry and properties of CRH3 train are given in Table 1. The train was assumed to traverse smoothly at a constant speed along the rail surface. This method was based on the large (finite) sliding contact model in ABAQUS, as shown in Figure 2, while the implicit direct time integration scheme was employed with automatic time increments. This integration was unconditionally stable to provide a better numerical convergence than explicit analysis in our case. Nonetheless, this type of integration involves large time step and high computational cost. The main strength of implicit time integration is that it can use static and dynamic analysis simultaneously. The time increment was calculated based on the high frequency of the FE model [22]. The resulted time increment ($\Delta t = 0.0015$) was set to the model to ensure the stability and accuracy of the implicit integration.

2.2. Track Model. In order to assess dynamic responses of the train-track-ground system, a CRTSI (China Railway Track System I) ballastless track was selected with standard gauge of 1.435 m, as shown in Figure 1. It is mainly composed of rail, fastening system, slab track, CA mortar layer, concrete base, roadbed, subgrade, and ground layers. However, in our case, the asphalt concrete trackbed was paved between base and roadbed layer. Due to the symmetry of the track in the moving direction, only half of the structure was generated in the simulation as depicted in Figure 3. For the simulation model, the length, width, and

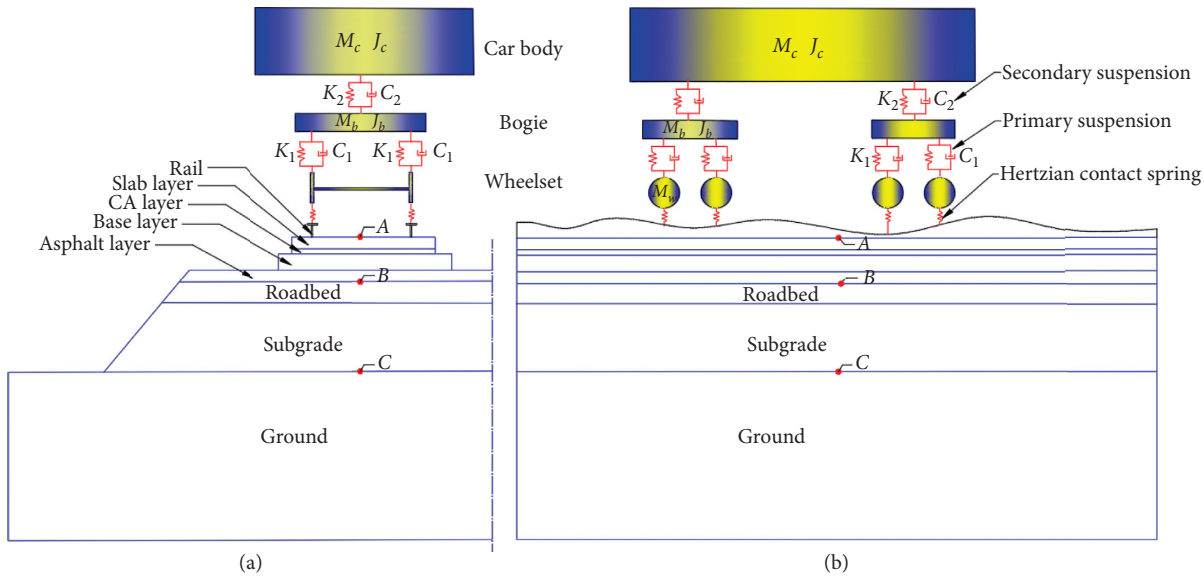

Figure 1: Representative view of the train-track-ground model together. Longitudinal view (a) and transversal view (b).

Table 1: Parameters of CRH3 high-speed train [26].

Parameters	Value
Mass of car body M_c (kg)	40000
Mass of bogie M_t (kg)	3200
Mass of wheel M_w (kg)	1200
Pitch inertia of car body J_c (kg·m^2)	5.47×10^5
Pitch inertia of bogie J_t (kg·m^2)	6800
Stiffness of primary suspension system K_1 (MN/m)	2.08
Stiffness of secondary suspension system K_2 (MN/m)	0.8
Damping of primary suspension system C_1 (kN·s/m)	100
Damping of secondary suspension system C_2 (kN·s/m)	120
Wheelbase 2 (m)	2.5
Distance between bogie centres 2 (m)	17.375
Length of vehicle (m)	25.675
Stiffness of wheel/rail contact Kc (MN/m)	1.325×10^3
Axle load (kN)	140

depth of the structure were set to 64 m × 45 m × 40 m, respectively. The track components were considered as a solid element. Because of rail existence in the FE model, the rail was assumed as rectangular cross section, while the spring and dashpot elements were employed to be located between the rail and slab layer to represent the rail pads, with a stiffness value of 60 MN/m and a damping coefficient of 47.7 kN·s/m [10]. Additionally, Tie constrains were used between two adjacent parts and "surface to surface" criteria were implemented.

It is common knowledge that in any FE analysis element size plays importantly influential factor in the results, in terms of accuracy and efficiency; therefore the element size was selected carefully without influencing on the results. The element size was determined according to a maximum frequency of incident motions and shear wave velocity of the structure [23], which can be set as 1/6–1/10 of the shortest wavelength. Sensitivity analysis has been done in a previous study of authors in order to obtain appropriate mesh size [10]. According to the sensitivity analysis, the maximum element size was set as 0.32 m for the structures. A non-uniform mesh was used for the ground structure and the total number of elements and nodes was 524038 and 599888, respectively. In order to select suitable finite element type, a sensitivity analysis was carried out. From the sensitivity analysis, eight-node linear-brick reduced integration elements and infinite elements were extracted. They proved to be most adequate for the problem. Later, infinite elements were discussed as well in the next subsection. Moreover, the calculation time of each model is about 85 h on a supercomputer with 64 GB RAM at 4.20 GHz with 24 processors.

2.3. Track Irregularity. Track irregularities impact significantly on dynamic responses of the train-track-ground system. Therefore, in order to obtain more realistic results, the track irregularities must be considered in detail for the simulations. In this study, only the random vertical irregularities were considered; lateral alignments were neglected. The random track irregularities are commonly described by using a one-side power spectrum density (PSD) function. The PSD function of the track spectrum for the Chinese Railway system can be defined through the following expression [24]:

$$S(f) = \frac{A\left(f^2 + Bf + C\right)}{f^4 + Df^3 + Ef^3 + Ff + G}, \quad (1)$$

where $S(f)$ is the power spectrum density and A, B, C, D, E, F, and G are the specific parameters, as presented in Table 2 and adopted from [25]. The vertical rail irregularities were employed as an input file to the simulation model by applying the amplitude of the irregularities to the coordinates of the nodes at the top of the rail. MATLAB® was employed in order to generate the rail irregularities. Figure 4 shows the vertical rail irregularities in the spatial domain.

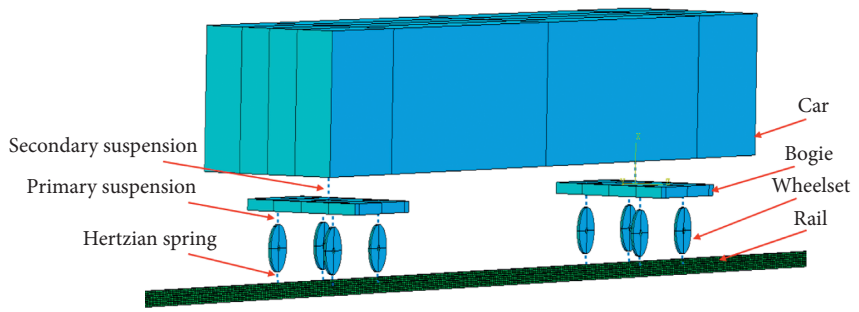

Figure 2: Representative view of the train model together with bogie and wheelset design.

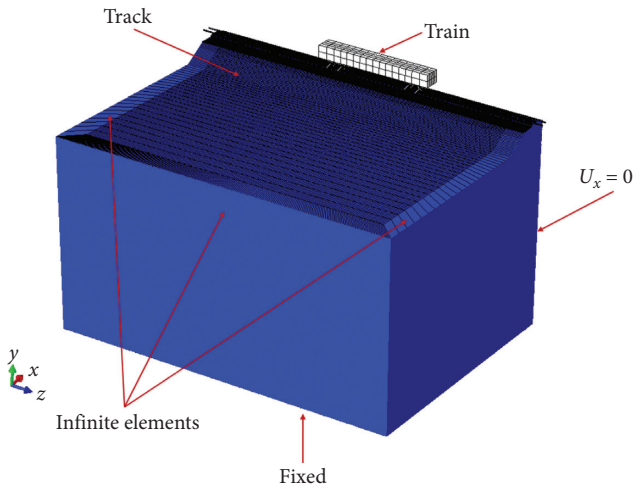

Figure 3: Symmetrical half model of the train-track-ground system.

2.4. Boundary Conditions. In FE analysis, one of the major issues when accomplishing dynamic analysis of the soil structure was the boundary condition. In other words, the standard (fixed) boundary conditions were unacceptable for this case due to unwanted reflections from the boundaries. In the FE model, viscous boundary conditions (infinite elements) are broadly used since they result in good stability and high accuracy [23, 27, 28]. This approach was engaged based on two series combinations of dashpot elements in the normal direction and a single dashpot element in the tangential direction at boundary nodes. This technique was applied in ABAQUS software. It could be expressed as follows:

$$\sigma = \rho \cdot c_p \cdot v_n, \tag{2}$$

$$\tau = \rho \cdot c_s \cdot v_t, \tag{3}$$

where ρ is material density; σ and τ are normal and shear stresses at the boundary, respectively; c_p and c_s are velocity of longitudinal and shear waves, respectively; v_n and v_t are velocities in the normal and tangential directions, respectively. The infinite elements were engaged on opposite sides of the symmetry plane and on the front and rear sides, in order to reduce wave reflection from boundary conditions here. A fixed boundary condition was employed at the bottom surface of the model. In a word, all degrees of freedom were restrained in every direction, as shown in Figure 3.

2.5. Modelling of Material Damping. The damping of the FE model could be modelled based on Rayleigh damping theory, which is also called as proportional damping. This damping is one of the most common ones that is used in dynamics analysis of energy dissipation. This approach has several advantages such as being simple, easy to use, and cost efficient. This could be described by designing the damping matrix $[C]$ as a linear combination of mass and stiffness matrices [29]. It can be described as follows:

$$[C] = \alpha[M] + \beta[K], \tag{4}$$

where $[M]$ and $[K]$ are mass and stiffness matrices, respectively, and α and β are called stiffness and mass proportional coefficients, respectively. These coefficients could be obtained by a natural frequency analysis of systems. Generally, most of the previous studies in research of dynamic response of the railway track structure have considered only damping of the soil layer, and other layers have been ignored. In fact, different structures have different natural frequencies, and they depend on elasticity and shape of the structure; therefore the natural frequency analysis must be done separately for each layer of the track system. In this study, the values of α and β were defined for the frequency range of 0.5–50 Hz for different layers. Rayleigh damping coefficients are identified in Table 3.

2.6. Material Characterization of Asphalt Concrete. The viscoelastic asphalt material behavior was taken into account for the simulation. In ABAQUS, the viscoelastic material was implemented with a generalized Maxwell method, in terms of a Prony series. The serial combination of one spring and one dashpot elements was engaged. The combination of the two elements was imitated as a linear viscoelastic model. Time dependency of the linear viscoelastic material characterization can be obtained from the following equation [30]:

$$G(t) = G_0\left(1 - \sum_{i=1}^{n} g_i\left(1 - e^{-(t/\tau_i)}\right)\right), \tag{5}$$

where $G(t)$ is the relaxation modulus at time t; G_0 is the instantaneous modulus; g_i is the Prony series parameter; τ_i is the relaxation time; and n is the number of parameters.

As it is well known, the viscoelastic material has the temperature dependency behavior. Thereby, the Williams-

Table 2: Parameters of the vertical track irregularities [24].

Parameters	A	B	C	D	E	F	G
Left rail vertical	1.1029	−1.4709	0.5941	0.8480	3.8016	−0.2500	0.0112
Right rail vertical	0.8581	−1.4607	0.5848	0.0407	2.8428	−0.1989	0.0094

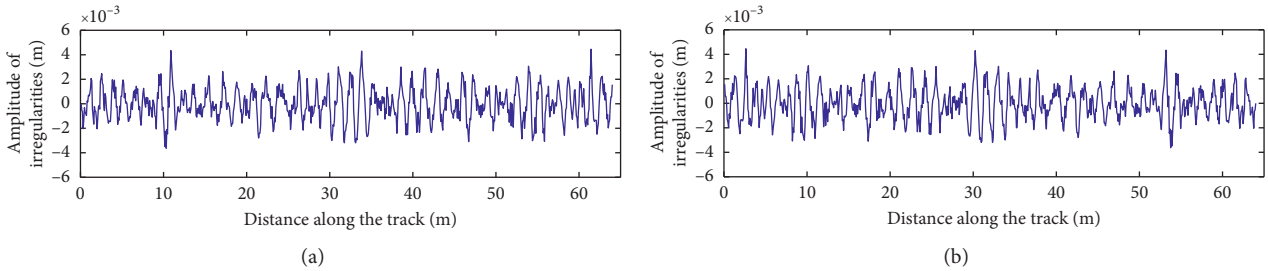

Figure 4: Vertical rail irregularities.

Table 3: Material parameters of the ballastless railway track [10].

Parts	Geometry (m)	Materials	Elastic modulus (Pa)	Poisson ratio	Density (kg/m^3)	Damping ratio	Rayleigh damping coefficients
Rail	UIC 60	Steel	2.06×10^{11}	0.030	7800	0.015	α 0.054 β 0.00094
Concrete slab	Width: 2.4 Thickness: 0.19	Cement concrete, C50	3.5×10^{10}	0.167	2450	0.030	α 0.105 β 0.016
CA layer	Width: 2.4 Thickness: 0.05	Cement, asphalt emulsion, and sand	4×10^{8}	0.167	2050	0.035	α 0.09 β 0.011
Concrete base	Width: 3 Thickness: 0.3	Cement concrete, C40	3.3×10^{10}	0.167	2300	0.030	α 0.16 β 0.00105
Roadbed	Width: 7.8 Thickness: 0.7	Crushed stone	1.5×10^{8}	0.250	2200	0.045	α 0.13 β 0.011
Subgrade	Width: 11.25 Thickness: 2.3	A and B filler and improved soil	0.6×10^{8}	0.250	2000	0.039	α 0.08 β 0.0925
Ground	Width: 45 Thickness: 40	A, B, and C filler and improved soil	0.5×10^{8}	0.330	1800	0.035	α 0.091 β 0.0083

Landel-Ferry equation [25] together with Prony series was employed to generate the temperature dependency behavior. It can be expressed as follows:

$$\log(a_T) = -\frac{C_1(T - T_0)}{C_2 + (T - T_0)}, \quad (6)$$

where T is test temperature; a_T is shift factor for temperature of T; T_0 is reference temperature; C_1 and C_2 are regression coefficients. The Prony series and shift factor parameters are provided in Table 4.

2.7. Validation of Numerical Approach. The proposed model was validated using an experimental test to verify the correctness and accuracy of the FE model. The experiments to acquire the vertical acceleration from the dynamic movements of high-speed train were performed on railway located in Shanghai-Nanjing. The experiment was focused on the vertical acceleration of track vibration on the CRTSI. The same conditions and variables set in the measurement were employed in the numerical model. In addition, the asphalt concrete trackbed was not paved in the substructure. Figure 5 shows the installation of test

Table 4: Viscoelastic parameters of asphalt material at 21°C [31].

i	τ_i	g_i
1	0.00001	0.3933
2	0.0001	0.2357
3	0.001	0.1867
4	0.01	0.1168
5	0.1	0.0438
6	1	0.0153
7	10	0.0044
8	100	0.0007
9	1000	0.0018
WLFT = 21	C_1	7.3
	C_2	93

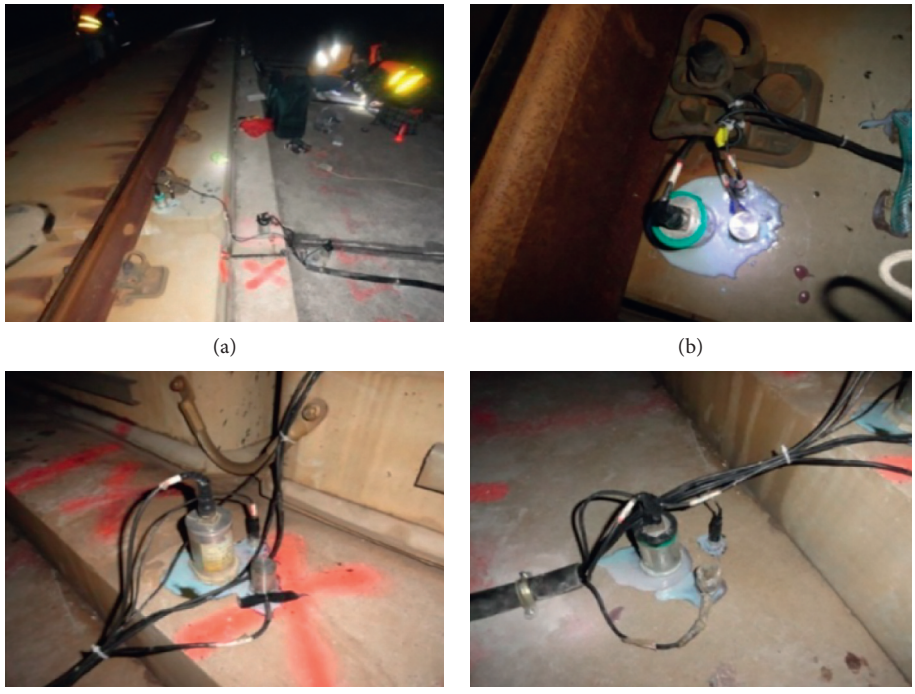

(a) (b) (c) (d)

Figure 5: Test sensors installation on the Shanghai-Nanjing railway line [32]. (a) Overall view. (b) On the slab layer. (c) On the base layer. (d) On the roadbed layer.

sensors on the CRTSI. The same sensors were used for the slab, base, and roadbed layers. During the test, the signals of all the sensors have been acquired via a dynamic acquisition system and transformed to the vibration acceleration. Further details about the field test can be found in [32].

With the aim of verifying the correctness of the model, the results, in terms of simulated vertical acceleration, were compared with the measured ones from the real-life test data. The comparison analyses were based on the root-mean-square (RMS) error percentage. The RMS errors highlight the absolute fitting between the simulated and measured ones. Taking into account the disregarded lateral, longitudinal forces and the errors in the modelling of the trackbed structure, the RMS error value of <20% was acceptable [33]. The RMS error can be formulated as follows:

$$\varepsilon_{\mathrm{RMS}} = \sqrt{\frac{1}{N}\left(\frac{\left(Z_{\mathrm{m}} - Z_{\mathrm{s}}\right)^2}{Z_{\mathrm{m}}}\right)} \cdot 100\%, \tag{7}$$

where Z_{m} and Z_{s} are the measured and simulated data, respectively, within the time of engaged for travelling the specified distance. N is the total number of samples in the measured and simulated data.

In addition to the correlation in time domain, frequency domain correlation, based on the coherence behavior of Power Spectrum Density (PSD) content of the simulated and measure acceleration [34], has been carried out to check if they produce the same wavelengths. The coherence value resulting from the frequency content of the datasets basically describes the relationship between two datasets. The coherence values range between 0 and 1. The highest value of coherence corresponds to highest correlation and other ways around. The threshold was chosen as 0.6 based on the same reason given above [35].

2.8. Evaluation of the Simulation Model Performances. Using the developed 3D model, various numerical investigations of the dynamic responses were carried out to examine the influence of various speeds, weather conditions (temperature), and asphalt trackbed thickness. This was conducted at three different points (A point, B point, and C point) in the midspan of longitudinal length of the track structure. The points A, B, and C were located on the slab layer, under the asphalt concrete trackbed and on the ground layer, respectively (as demonstrated in Figure 1). As the train speed is the key factor in influencing the dynamic responses of the railway structure, the vertical acceleration-time history curves at the different points of the entire structure considering various speeds were evaluated. For the evaluation, the temperature of 25°C and 15 cm of asphalt trackbed thickness were set as reference parameters.

In next step, running the model was performed with the same procedure as above, but including different temperatures in the developed model to see its influence on dynamic responses of the railway structure, in terms of its vertical acceleration. It is because of the assumed viscoelastic behavior of asphalt material in the model. Four temperature of −10°C, 5°C, 25°C, and 45°C were applied and the thickness of the asphalt concrete trackbed was kept at 15 cm at the points of A, B, and C. For all four sceneries, the speed was kept constant (350 km·h^{-1}).

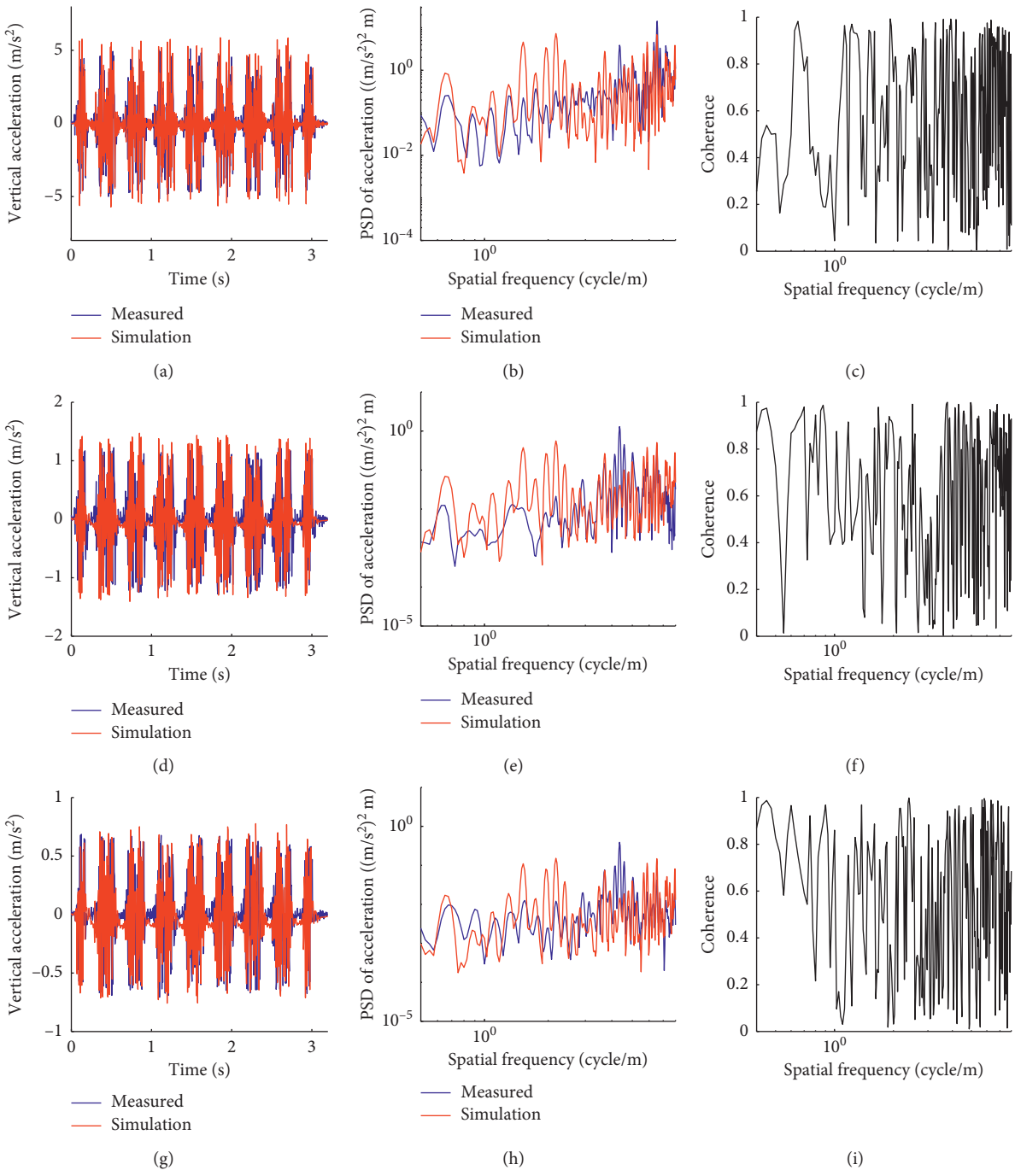

Figure 6: The simulated and measured acceleration (a, d, and g), the PSD content (b, e, and h), and corresponding coherence (c, f, and i) on the slab layer, on the base layer, and on the roadbed layer, respectively.

One of very common approaches for minimizing the dynamic responses of the trackbed to the train motion is to enhance the thickness of the asphalt concrete trackbed, due to the bending stiffness and mass of the trackbed structure. Thereby, in the final step, the effects of different thickness with size 0 cm, 7 cm, 15 cm, and 22 cm of the asphalt concrete trackbed were evaluated. The speed of the train and the applied temperature were set as constant with the value of 350 km·h^{-1} and 25°C. Additionally, the width and length of asphalt concrete trackbed were held constant.

3. Results and Discussions

3.1. Validation of the Simulation Model. The developed simulation model was run by implementing the equations from (1) to (7) in ABAQUS by considering all the necessary parameters. The time domain and frequency content (PSD) together with its corresponding coherence pattern of the simulated and measured accelerations were demonstrated in Figure 6. The analyses of the correlation in the time domain (Figures 6(a), 6(d), and 6(g)) depicted a good agreement

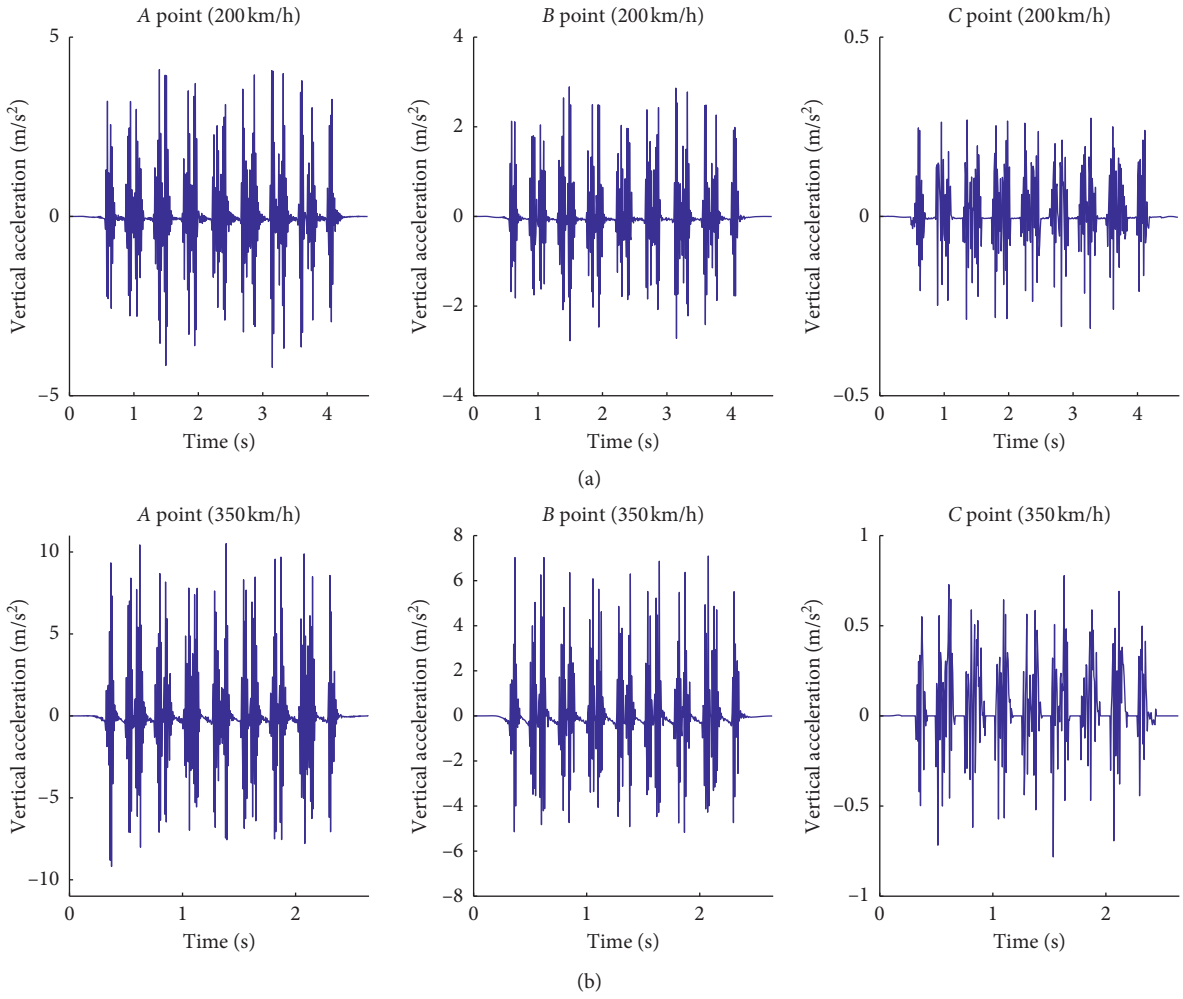

Figure 7: The simulated vertical accelerations at the points A, B, and C with the train speed 200 and 350 km·h^{-1}.

between the simulated and measured data at the train speed of 245 km·h^{-1} with RMS error of 11%, 9%, and 10% on the slab, on the base, and on the roadbed layers, respectively. The investigation of the frequency content also indicted a well correlation with the average value of 0.68, 0.7, and 0.69, on the slab, on the base, and on the roadbed layers, respectively. Considering the RMS error below the threshold error and the coherence value above the threshold, it can be outlined that the proposed simulation model is fully capable of simulating the dynamic responses of the train-track-ground coupling system.

3.2. Influence of Train Speed on Dynamic Responses. The simulated vertical accelerations at the three-observation point of the structure (A, B, and C) with the constant speed of 200 and 350 km·h^{-1} were shown in Figure 7. From the qualitative analyses, a considerable difference in vertical accelerations, in terms of the dynamic response of the trackbed, which resulted from different train speed can be noticed. Furthermore, as the train speed increased, the amplitudes of the vertical acceleration dramatically rose at all observation points (A, B, and C). As it was expected, there was a decrease in the vertical acceleration magnitudes from A to C point for both speeds, due to the geometrical damping of structures and internal damping of asphalt concrete trackbed.

In order to define quantitatively the influence of the specified train speeds on the dynamic responses, the maximum values of the resultant vertical accelerations were estimated; see Figure 8. The estimation indicated that, at point A, the maximum amplitude of vertical acceleration was approximately 4.1 m· s^{-2} for the speed of 200 km·h^{-1}. Comparison of this with the maximum value of the vertical acceleration at a speed of 350 km·h^{-1} indicated that there was rise of almost 151%. The same patterns were observed for point B and point C with the increase of 116% and 153%, respectively. The mean value estimation highlighted a gradual decrease from A to B with the values of 6.9, 4.81, and 0.54 m·s^{-2}, respectively.

Based on the above-carried analyses of the determined results, it can be stated that the train speed significantly influences the dynamic responses and thus needs to be carefully considered in designing the railway substructure.

3.3. Temperature Effects. Figure 9 demonstrated the patterns of the vertical acceleration for the lowest and highest temperatures of −10°C and 45°C, respectively, at the points A, B, and C. From the qualitative analyses, the same patters

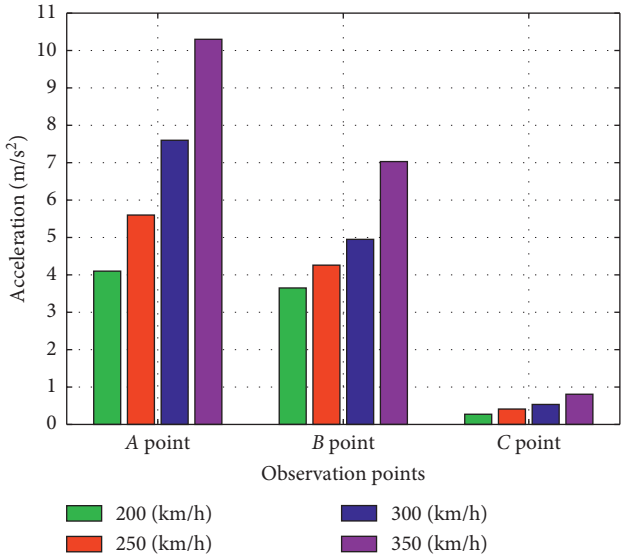

Figure 8: The speed effect on the vertical accelerations at the observation points of A, B, and C.

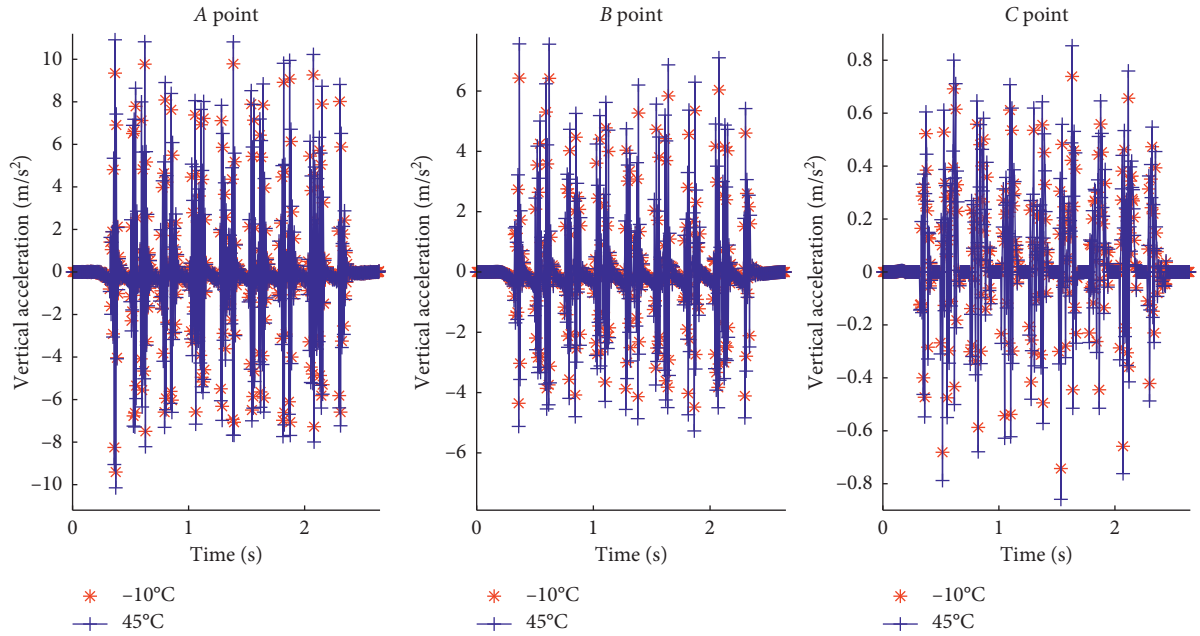

Figure 9: The simulated vertical acceleration under the temperature of −10°C and 45°C with the speed of 350 km·h^{-1}.

as above for the changes in the vertical accelerations could be captured. Therefore, the maximum magnitude of the vertical acceleration affected by all four applied temperature was analyzed. This showed that there was a growth of 17.2% in the values of the acceleration (from 9.3 to 10.9 m·s^{-2}) at the point A, as the temperature shifts up from −10°C to 45°C. The figure for the growth percentage was the same with value of 17.2% for the points B and C.

In addition to the above-given analyses, the mean values of the vertical acceleration which resulted from all three point of observation (Figure 10) were also defined for each applied temperature. The determined mean values were approximately 5.48 m·s^{-2}, 5.7 m·s^{-2}, 6.04 m·s^{-2}, and 6.42 m·s^{-2} at the temperature of −10°C, 5°C, 25°C, and 45°C, respectively. Based on the defined mean values, the correlation between the temperature and acceleration, in terms of increasing pattern of both parameters, could be noticed at all three-observation points. This confirmed the fact once more that the modulus and viscous coefficient of asphalt material decreased with increase of the temperature. Overall, considering all of the conducted analysis for the temperature effects, the temperature was also one of the major factors affecting the dynamic responses of the asphalt concrete trackbed.

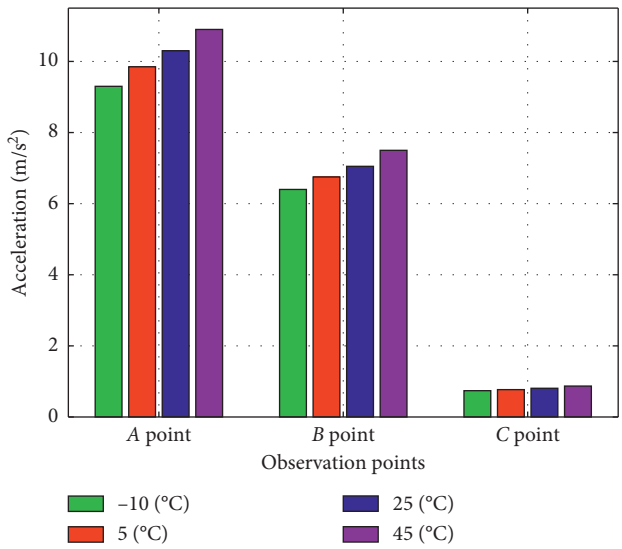

Figure 10: The temperature effect on the vertical accelerations at all observation points with the speed of 350 km·h^{-1}.

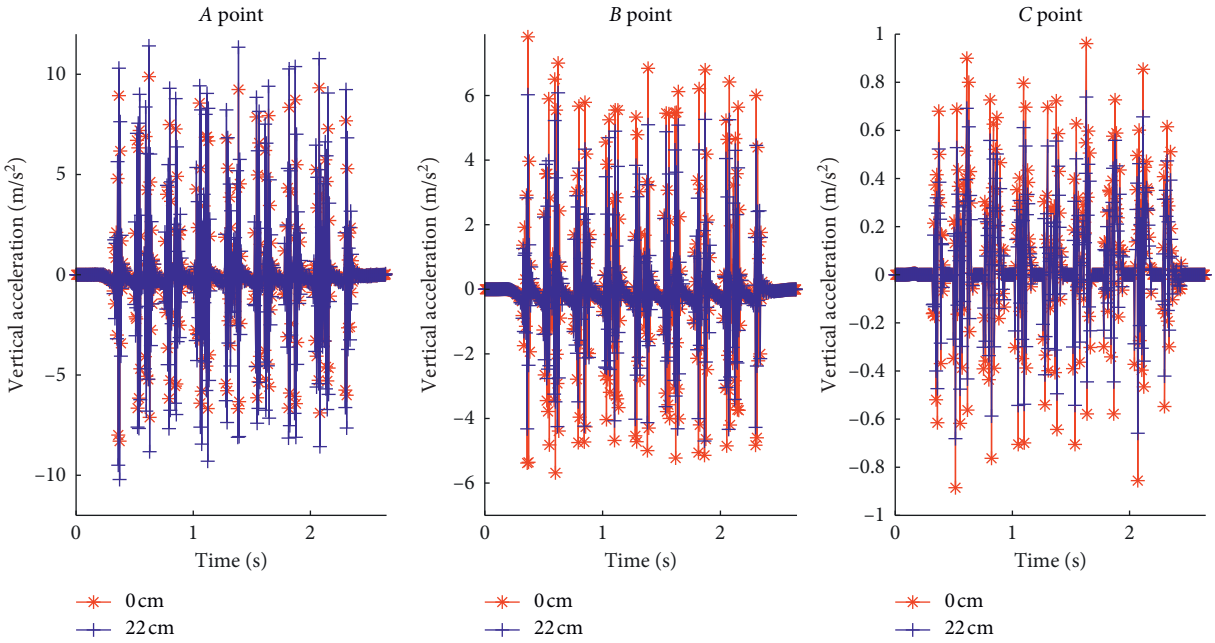

Figure 11: The simulated vertical acceleration with the thickness of 0 cm and 22 cm at the observation points A, B, and C.

3.4. Thickness of the Asphalt Concrete Trackbed versus Its Dynamic Responses. Figure 11 presents the vertical acceleration-time history curves produced by simulating the asphalt concrete trackbed with the thickness of 0 cm and 22 cm. Two more of thickness size included in the simulation were considered in the further analyses of the maximums of the simulated acceleration; see Figure 12. At point A, the vertical acceleration of the trackbed with the thickness of 0 cm, 8 cm, 15 cm, and 22 cm indicated an upward trend with maximum amplitude of around 9.5 m·s^{-2}, 9.7 m·s^{-2}, 10.2 m·s^{-2}, and 11.1 m·s^{-2}, respectively. This drew the total increase of 16.8% between the applied thickness from 0 cm to 22 cm. Moreover, the upward trend rises considerably after thickness of 15 cm. Therefore, the recommended thickness of the asphalt concrete trackbed would be equal to 15 cm. This revealed that the increase in the thickness of asphalt concrete trackbed at the point A caused the accelerated response, in terms of higher amplitudes of the vertical acceleration on the slab layer. The main reason lies in the fact that the stiffness of the track structure increases as the thickness of asphalt concrete trackbed increases. As a result, it will cause excessive acceleration in the upper layers. This was also found by other researchers [9, 36]. However, at points B and C, the vertical acceleration experienced a reverse trend compared to the point A. It is because the mass of the structure grows with the growing thickness of the asphalt concrete trackbed, which is proportional of the damping. It can be proposed that the

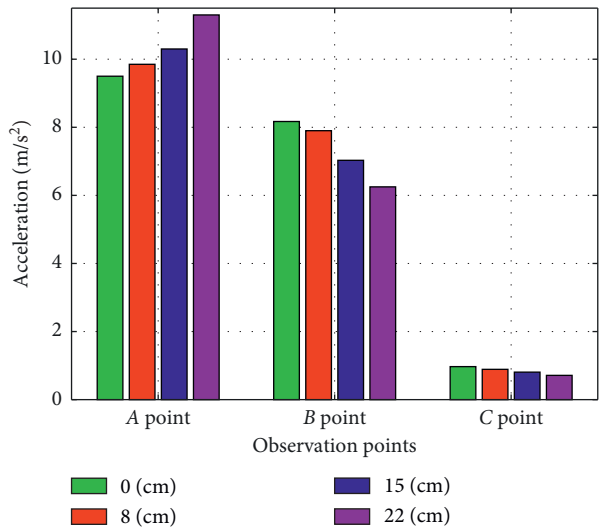

Figure 12: The amplitudes of the vertical accelerations at all the observation points versus various thickness.

stiffness and the mass of the structure need to be balanced in order to achieve an optimal thickness of the asphalt concrete trackbed. At points B and C, the maximums of the accelerations at the layer thickness of 0 cm, 8 cm, 15 cm, and 22 cm went down with the values of 8.17 m·s^{-2}, 8.02 m·s^{-2}, 7.03 m·s^{-2}, and 6.2 m·s^{-2}, respectively. The same pattern was observed at point C. The total shift down in percentage for the points B and C was equal to 24.1% and 26.8%, respectively.

The first overview from these analyses was that the higher thickness resulted in improved dynamic responses, in terms of the acceleration amplitudes, of the asphalt concrete trackbed, except for the point A. However, the cost and settlement of the structure for increasing the thickness of asphalt concrete trackbed need to be taken into account.

4. Conclusions

A dynamics model for the vertical coupling of the train-track-ground system was developed based on finite element method in ABAQUS. The main features of this model involved the linear effects of the coupling system between the train and track considering the rail irregularities and viscoelastic behavior of the asphalt material. However, the only limitation of the model was the incapacity of simulating the horizontal dynamics. The effects of different train speeds, thickness of the asphalt concrete trackbed, and temperature to the dynamic responses were analyzed and evaluated to examine the effectiveness of the asphalt concrete trackbed. The findings of these analyses and evaluations could be used to enhance the asphalt concrete trackbed design in the railway substructure. The following conclusions and future work recommendations were drawn from this study.

(1) Based on the FE results, the proposed model has a strong capability of simulating the vertical dynamic responses of the train-track-ground coupling system with a sufficient accuracy.

(2) According to the parametric analysis, the increase of train speed caused significant elevation on the dynamic responses at all the selected points.

(3) The temperature effects on the dynamic responses of the trackbed should be considered while designing the trackbed structure since the railway track was witnessed with the greater acceleration at all the selected points with the rise of the temperature.

(4) The analyses of the asphalt concrete tracked thickness versus the dynamic responses of the railway structure also confirmed that the increasing of the thicknesses lowered the amplitude of the vertical acceleration resulting in a better dynamic response after at the point of B and C of the designed asphalt concrete trackbed.

(5) According to the results of parametric analysis, a thickness of asphalt concrete trackbed of 15 cm is recommended.

(6) The model proved to be valuable for the further experimental examinations of the influence of the asphalt concrete trackbed on the ground born vibrations generated by high-speed train.

Data Availability

Other data used to support the findings of this study are available from the corresponding author upon request.

Conflicts of Interest

The authors declare that there are no conflicts of interest regarding the publication of this paper.

Acknowledgments

This research was jointly and financially supported by the Fundamental Research Funds for the Central Universities under Grant 2682019ZT05 and by the National Basic Research Program of China (NSFC) under Grant 51778541. The authors also would like to express their gratitude to Dr J. Huang from Southwest Jiaotong University (Chengdu, China) for sharing the experimental data.

References

[1] J. Xue-song, "Key problems faced in high-speed train operation," *Journal of Zhejiang University SCIENCE A*, vol. 15, no. 12, pp. 936–945, 2014.

[2] H. Gou, Z. Ran, L. Yang, Y. Bao, and Q. Pu, "Mapping vertical bridge deformations to track geometry for high-speed railway," *Steel and Composite Structures*, vol. 32, no. 4, pp. 467–478, 2019.

[3] H. Gou, H. Long, Y. Bao, G. Chen, and Q. Pu, "Dynamic behavior of hybrid framed arch railway bridge under moving trains," *Structure and Infrastructure Engineering*, vol. 15, no. 8, pp. 1015–1024, 2019.

[4] X. Sheng, "A review on modelling ground vibrations generated by underground trains," *International Journal of Rail Transportation*, vol. 7, no. 4, pp. 1–21, 2019.

[5] G. Kouroussis, D. P. Connolly, and O. Verlinden, "Railway-induced ground vibrations—a review of vehicle effects," *International Journal of Rail Transportation*, vol. 2, no. 2, pp. 69–110, 2014.

[6] E. Yang, K. C. P. Wang, Q. Luo, and Y. Qiu, "Asphalt concrete layer to support track slab of high-speed railway," *Transportation Research Record: Journal of the Transportation Research Board*, vol. 2505, no. 1, pp. 6–14, 2015.

[7] E. Yang, K. C. P. Wang, Y. Qiu, and Q. Luo, "Asphalt concrete for high-speed railway infrastructure and performance comparisons," *Journal of Materials in Civil Engineering*, vol. 28, no. 5, Article ID 04015202, 2016.

[8] M. Fang, Y. Qiu, C. Ai, and Y. Wei, "Gradation determination of impermeable asphalt mix on subgrade surface layer for ballastless track in high-speed railway lines," in *Proceedings of the Third International Conference on Transportation Engineering ICTE*, pp. 1926–1931, ASCE, Chengdu, China, July 2011.

[9] J. C. Wang, X. Zeng, and R. L. Mullen, "Three-dimensional finite element simulations of ground vibration generated by high-speed trains and engineering countermeasures," *Journal of Vibration and Control*, vol. 11, no. 12, pp. 1437–1453, 2005.

[10] B. Yusupov, Y. Qiu, H. Ding, and A. Rahman, "Temperature and material behaviour effects on dynamic responses of asphalt concrete trackbed," *International Journal of Rail Transportation*, vol. 8, no. 1, pp. 1–14, 2019.

[11] S. Liu, J. Yang, X. Chen, G. Yang, and D. Cai, "Application of mastic asphalt waterproofing layer in high-speed railway track in cold regions," *Applied Sciences*, vol. 8, no. 5, p. 667, 2018.

[12] S.-H. Lee, D.-W. Park, H. V. Vo, and M. Fang, "Analysis of asphalt concrete track based on service line test results," *Construction and Building Materials*, vol. 203, pp. 558–566, 2019.

[13] Z. Yu, D. P. Connolly, P. K. Woodward, and O. Laghrouche, "Settlement behaviour of hybrid asphalt-ballast railway tracks," *Construction and Building Materials*, vol. 208, pp. 808–817, 2019.

[14] S.-H. Lee, Y.-T. Choi, H.-M. Lee, and D.-W. Park, "Performance evaluation of directly fastened asphalt track using a full-scale test," *Construction and Building Materials*, vol. 113, pp. 404–414, 2016.

[15] S.-H. Lee, J.-W. Lee, D.-W. Park, and H. V. Vo, "Evaluation of asphalt concrete mixtures for railway track," *Construction and Building Materials*, vol. 73, pp. 13–18, 2014.

[16] S.-H. Lee, D.-W. Park, H. V. Vo, and S. Dessouky, "Asphalt mixture for the first asphalt concrete directly fastened track in Korea," *Advances in Materials Science and Engineering*, vol. 2015, Article ID 701940, 6 pages, 2015.

[17] J. G. Rose, P. F. Teixeira, and N. E. Ridgway, "Utilization of asphalt/bituminous layers and coatings in railway trackbeds: a compendium of international applications," in *Proceedings of the Joint Rail Conference*, vol. 1, no. 49064, pp. 239–255, Urbana, IL, USA, April 2010.

[18] J. G. Rose, S. Liu, and R. R. Souleyrette, "KENTRACK 4.0: a railway trackbed structural design program," in *Proceedings of the Joint Rail Conference*, no. 45356, Colorado Springs, CO, USA, April 2014.

[19] Q. Li, H. Ding, A. Rahman, and D. He, "Evaluation of basic oxygen furnace (BOF) material into slag-based asphalt concrete to be used in railway substructure," *Construction and Building Materials*, vol. 115, pp. 593–601, 2016.

[20] Y. Liu, Z.-d. Qian, D. Zheng, and Q.-b. Huang, "Evaluation of epoxy asphalt-based concrete substructure for high-speed railway ballastless track," *Construction and Building Materials*, vol. 162, pp. 229–238, 2018.

[21] H. Gou, Y. He, W. Zhou, Y. Bao, and G. Chen, "Experimental and numerical investigations of the dynamic responses of an asymmetrical arch railway bridge," *Proceedings of the Institution of Mechanical Engineers, Part F: Journal of Rail and Rapid Transit*, vol. 232, no. 9, pp. 2309–2323, 2018.

[22] R. Courant, K. Friedrichs, and H. Lewy, "On the partial difference equations of mathematical physics," *IBM Journal of Research and Development*, vol. 11, no. 2, pp. 215–234, 1967.

[23] J. Y. Shih, D. J. Thompson, and A. Zervos, "The effect of boundary conditions, model size and damping models in the finite element modelling of a moving load on a track/ground system," *Soil Dynamics and Earthquake Engineering*, vol. 89, pp. 12–27, 2016.

[24] W. Zhai, K. Wang, and C. Cai, "Fundamentals of vehicle—track coupled dynamics," *Vehicle System Dynamics*, vol. 47, no. 11, pp. 1349–1376, 2009.

[25] M. L. Williams, R. F. Landel, and J. D. Ferry, "The temperature dependence of relaxation mechanisms in amorphous polymers and other glass-forming liquids," *Journal of the American Chemical Society*, vol. 77, no. 14, pp. 3701–3707, 1955.

[26] X. Lei and B. Zhang, "Analysis of dynamic behavior for slab track of high-speed railway based on vehicle and track elements," *Journal of Transportation Engineering*, vol. 137, no. 4, pp. 227–240, 2011.

[27] J. Lysmer and R. Kuhlemeyer, "Finite dynamic model for infinite media," *Journal of the Engineering Mechanics Division*, vol. 95, no. 4, pp. 859–877, 1969.

[28] Y. B. Yang and H. H. Hung, "A 2.5D finite/infinite element approach for modelling visco-elastic bodies subjected to moving loads," *International Journal for Numerical Methods in Engineering*, vol. 51, no. 11, pp. 1317–1336, 2001.

[29] A. K. Chopra, *Dynamics of Structures*, Prentice Hall, Upper Saddle River, NJ, USA, 2nd edition, 2001.

[30] J. D. Ferry, *Viscoelastic Properties of Polymers*, John Wiley & Sons, Hoboken, NJ, USA, 3rd edition, 1980.

[31] D. Zejiao, T. Yiqiu, and L. Meili, "Design and implementation of a full-scale accelerated pavement testing facility for extreme regional climates in China," in *Advances in Pavement Design through Full-Scale Accelerated Pavement Testing*, CRC Press, Boca Raton, FL, USA, 2012.

[32] J. Huang, Q. Su, T. Liu, and W. Wang, "Behavior and control of the ballastless track-subgrade vibration induced by high-speed trains moving on the subgrade bed with mud pumping," *Shock and Vibration*, vol. 2019, Article ID 9838952, 14 pages, 2019.

[33] H. M. Ngwangwa and P. S. Heyns, "Application of an ANN-based methodology for road surface condition identification on mining vehicles and roads," *Journal of Terramechanics*, vol. 53, pp. 59–74, 2014.

[34] G. M. Sharipov, D. S. Paraforos, A. S. Pulatov, and H. W. Griepentrog, "Dynamic performance of a no-till seeding assembly," *Biosystems Engineering*, vol. 158, pp. 64–75, 2017.

[35] J. H. Miles, "Estimation of signal coherence threshold and concealed spectral lines applied to detection of turbofan engine combustion noise," *The Journal of the Acoustical Society of America*, vol. 129, no. 5, pp. 3068–3081, 2011.

[36] H. Huang, S. Shen, and E. Tutumluer, "Moving load on track with asphalt trackbed," *Vehicle System Dynamics*, vol. 48, no. 6, pp. 737–749, 2010.